Influence of charge and flexibility on smectic phase formation in filamentous virus suspensions

Kirstin R. Purdy and Seth Fraden

Complex Fluids Group, Martin Fisher School of Physics, Brandeis University, Waltham, Massachusetts 02454, USA
(Received 22 January 2006; revised manuscript received 7 June 2007; published 17 July 2007)

We present experimental measurements of the cholesteric-smectic phase transition of suspensions of charged semiflexible rods as a function of rod flexibility and surface charge. The rod particles consist of the bacteriophage M13 and closely related mutants, which are structurally identical to M13, but vary either in contour length and therefore ratio of persistence length to contour length, or surface charge. Surface charge is altered in two ways; by changing solution pH and by comparing M13 with fd virus, a virus which differs from M13 only by the substitution of a single charged amino acid for a neutral one per viral coat protein. Phase diagrams are measured as a function of particle length, particle charge, and ionic strength. The experimental results are compared with existing theoretical predictions for the phase behavior of flexible rods and charged rods.

I. INTRODUCTION

In a suspension of hard or charged rods, purely repulsive entropic interactions are sufficient to induce liquid crystal ordering. Theory predicts that hard rods should exhibit isotropic, nematic, smectic, and columnar liquid crystal phases with increasing concentration [1–3]. Unfortunately, laboratory production of hard, rigid, monodisperse rods of colloidal dimensions is very difficult. Rigid and flexible polyelectrolyte macromolecular rods, however, are abundant, especially in biological systems, which by nature lend themselves to mass production. In this paper we will study the influence of flexibility and electrostatic interactions on the formation of a smectic phase from a nematic phase using suspensions of charged, semiflexible fd and M13 virus rods. Viruses, such as fd, M13, and tobacco mosaic virus are a unique choice for use in studying liquid crystal phase behavior in that they are biologically produced to be monodisperse and are modifiable by genetic engineering and post-expression chemical processing. These virus particles and $\beta-$FeOOH rods are, to our knowledge, the only colloidal systems known to exhibit the predicted hard-rod phase progression from isotropic (I) to nematic (N) or cholesteric to smectic (S) phases with increasing rod concentration [4–6]. Even though qualitative theories have been developed to describe either the effects of electrostatics or the effects of flexibility on the nematic-smectic (N-S) phase transition of hard rods [7–10], they have yet to be thoroughly tested experimentally. By measuring the N-S transition of charged, flexible rods we learn about both the influence of these parameters on smectic phase formation and the interactions between these rods in concentrated suspensions. Additionally, our results add insight into the ordering of other important rodlike polyelectrolytes such as DNA, which often appears in high concentrations under physiological conditions and exhibits cholesteric and columnar, but not smectic, liquid crystalline phases [11,12].

In this paper we test the limits of current theoretical predictions for the nematic-smectic phase transition in three ways. First, we measure the phase transition for semiflexible filamentous virus of identical structure and varied length. By changing the rod length and leaving local particle structure constant, the persistence length P of the rods, defined as the length over which tangent vectors along a polymer are correlated [13], remains constant. Subsequently, the rod flexibility, as defined by the ratio of persistence length to contour length L, or P/L, is altered. In our experiments the flexibility of the particles remains within the semiflexible limit, meaning $P \sim L$. Altering the particle flexibility within the semiflexible limit probes the competition between rigid and flexible rod phase behavior. Second, we vary the ionic strength of the virus rod suspensions allowing us to probe the efficacy of theoretical approximations for incorporating electrostatic repulsion into hard-particle theories. Third, we measure the nematic-smectic phase transition for filamentous virus of different charge. Altering the surface charge by two independent techniques, solution chemistry and surface chemistry, probes the importance of the details of the surface charge distribution in determining long range interparticle interactions. By varying these three independent variables, length, charge, and solution ionic strength, we systematically examine how electrostatic interactions and flexibility experimentally effect the nematic-smectic phase boundary.

The colloidal rods we use are the rodlike semiflexible bacteriophages fd and M13 which form isotropic, cholesteric (nematic), and smectic phases in solution with increasing virus concentration [8,14–16]. The free energy difference between the cholesteric and nematic phases is small, and therefore it is appropriate to compare our results with predictions for the nematic phase [17]. M13 and fd are composed of 2700 major coat proteins helicoidally wrapped about the single stranded viral DNA. They differ from one another by only one amino acid per major coat protein; the negatively charged aspartate (asp_{12}) in fd is substituted for the neutral asparagine (asn_{12}) in M13 [18]. These viruses are thus ideal for use in studying the charge dependence of the virus rod phase transitions. Changes in the surface charge of the particles were also achieved by varying the pH of the solution [19]. Additionally, by varying the length of the M13 DNA we created M13 mutants which differ only in contour length. The M13 mutants have the same local structure, and thus we assume persistence length, as M13. These mutant M13 viruses were used to measure the flexibility dependence of the nematic-smectic phase transition.

II. ELECTROSTATIC INTERACTIONS

For colloidal rods, the total rod-rod interparticle interaction includes a combination of hard core repulsion and long ranged electrostatic repulsion. To our knowledge there are only two theories which attempt to incorporate electrostatic interactions into hard-rod theories for the nematic-smectic phase transition, both of which are based on the calculation of an effective hard-core diameter (D_{eff}) which is larger than the bare diameter D. The first originates from Onsager's calculation of the second virial coefficient of the free energy for charged rods in the isotropic phase [1,20]. The second was developed by Kramer and Herzfeld who calculate an *avoidance diameter* which minimizes the scaled particle expression for the free energy of charged parallel spherocylinders as a function of concentration [7]. In this paper, we will predominantly use Onsager's D_{eff} to model the electrostatic interactions of our charged rods because the accuracy of using D_{eff} to incorporate electrostatic interactions into hard-flexible rod theory has been experimentally verified for the isotropic-nematic phase transition [15,21]. However, we present a brief background of both theories in this section as they both have specific advantages and drawbacks.

For hard, rigid, rodlike particles, the limit of stability of the isotropic phase against a nematic phase is given by the Onsager relation $bc_i = 4$ where $b = \pi L^2 D/4$ and c_i is the isotropic number density of rods [1]. For charged particles, Onsager showed that the stability condition remains unchanged provided D is replaced with D_{eff}, thus $b_{eff}c_i = 4$, with $b_{eff} = \pi L^2 D_{eff}/4$. Increasing ionic strength decreases D_{eff}, and for highly charged colloids, such as M13 and *fd*, D_{eff} is nearly independent of surface charge due to the nonlinear nature of the Poisson-Boltzmann equation, which leads to counterion condensation near the colloid surface [15]. In previous work [15,21], the prediction that $b_{eff}c_i$ is constant at the *I-N* phase boundary has been experimentally verified at high ionic strength ($I > 60$ mM, large L/D_{eff}) for our system of semiflexible virus rods, as illustrated in Fig. 1. This validated the mapping of the *I-N* transition of charged virus rods at high ionic strength onto a hard-rod theory by using an effective hard diameter, D_{eff}. At low ionic strength ($I < 60$ mM), the prediction that $b_{eff}c_i$ is constant did not hold because of the breakdown of the second virial approximation at small L/D_{eff} [21]. Even so, the discrepancy between theory and experiment at low ionic strength was only about 30% for 5 mM $< I < 60$ mM. In this paper we will test the hypothesis that hard-rod theories of the *N-S* transition can be used to analyze experiments on charged rods by mapping the hard-rod diameter D to the effective diameter D_{eff}. We expect that this mapping will work (at best) only at high ionic strengths.

Since D_{eff} is valid only when the second virial approximation is valid, i.e. in the isotropic phase, Stroobants *et al.* developed an approximate way to describe the electrostatic interactions in the nematic phase using this second virial approximation [23]. They defined a nematic effective diameter D_{eff}^N, which is calculated from the isotropic effective diameter D_{eff}: $D_{eff}^N = D_{eff}[1 + h\eta[f]/\rho[f]]$, where $\rho[f] = \frac{4}{\pi}\langle\langle\sin\phi\rangle\rangle$ and $\eta[f] = \frac{4}{\pi}\langle\langle-\sin\phi\log(\sin\phi)\rangle\rangle - (\log(2) - 1/2)\rho[f]$. The average $\langle\langle\ldots\rangle\rangle$ is over the solid angle Ω
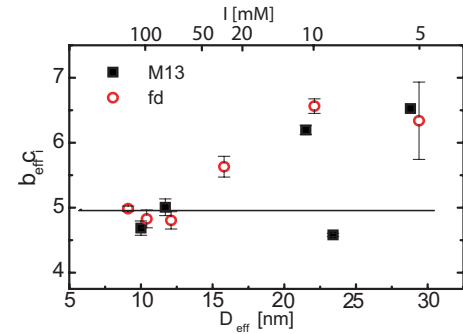

FIG. 1. (Color online) Isotropic-nematic phase transition $b_{eff}c_i$ plotted as a function of D_{eff} for both M13 and *fd* suspensions in Tris-HCl buffer at pH 8.2. The original data for this figure was published previously [21]. The solid line is the hard-rod prediction for semiflexible rods with a persistence length of 2.2 μm [22]. For small values of D_{eff} (high ionic strength), the coexistence concentrations for the charged rods are effectively mapped to the hard-rod predictions. The ionic strength scale is for *fd* suspensions (M13 has a lower surface charge, thus D_{eff} at the same ionic strength is slightly larger).

weighted by the nematic angular distribution function $f(\Omega)$ with ϕ describing the angle between adjacent rods [20]. The parameter $h = \kappa^{-1}/D_{eff}$, where κ^{-1} is the Debye screening length, characterizes the preference of charged rods for twisting. Crossed charged rods have a lower energy than parallel charged rods, and h correspondingly increases with increasing electrostatic interactions (decreasing ionic strength). This definition for the nematic effective diameter is accurate as long as the average angle between the rods and the nematic director $\sqrt{\langle\theta^2\rangle}$ is much greater than D_{eff}^N/L [24]. In this limit, the second virial coefficient is still much larger than the higher virial coefficients, which can be neglected. Near the *N-S* transition the order parameter, as determined by x-ray measurements of magnetically aligned samples, is $S = 0.94$ [25]. Using an angular distribution function with this order parameter of $S = 0.94$ we find that $D_{eff}^N = 1.16D_{eff}$ at 5 mM ionic strength and $D_{eff}^N = 1.10D_{eff}$ at 150 mM ionic strength. This corresponds to $\sqrt{\langle\theta^2\rangle} \sim 6D_{eff}^N/L$ for the largest value of D_{eff}^N.

Previously, we argued that D_{eff}^N, which is independent of virus concentration, could describe the electrostatic interactions of *fd* virus suspensions at the nematic-smectic transition [8]. However, as mentioned above, the use of D_{eff} beyond the regime where the second virial coefficient quantitatively describes the system is not justified, and from our calculation of $\sqrt{\langle\theta^2\rangle}$ we know the use of the second virial approximation is questionable. In this article, we probe an expanded range of measurements of the *N-S* transition of virus suspensions as a function of ionic strength, virus length, and virus surface charge to further test the robustness of the second virial coefficient approximation.

An alternative method for incorporating electrostatics into a hard-rod theory for the *N-S* transition was developed by Kramer and Herzfeld. They calculate an avoidance diameter D_a which minimizes the scaled particle expression for the free energy of charged parallel spherocylinders as a function of concentration [7]. With respect to ionic strength, D_a ex-

hibits the same trend as D_{eff}, but unlike D_{eff}, D_a is inherently concentration dependent, decreasing with increasing rod concentration. D_a is constrained to be always less than the actual rod separation, while D_{eff} is not so constrained. This can lead to the un-physical situation where D_{eff} is greater than the particle separation. Furthermore, by using the scaled particle theory, the avoidance diameter description accounts for third and higher virial coefficients in an approximate way, which is appropriate for the high concentrations of the nematic-smectic transition [26,27]. One disadvantage with the free energy expression developed by Kramer and Herzfeld is that it does not reduce to Onsager's theory in the absence of electrostatic interactions. Nevertheless, Kramer and Herzfeld's calculations also qualitatively reproduce previously published data for the *N-S* transition of *fd* virus [7].

III. MATERIALS AND METHODS

Wild type (*wt*) *fd* and M13 have length $L_{wt}=0.88$ μm, diameter $D=6.6$ nm, persistence length $P=2.2$ μm [5], and mass density $\rho_o=1.3$ g/ml [28]. The M13 mutants have the same diameter as the wild type M13 and lengths L of 1.2, 0.64, and 0.39 μm [16]. Because the molecular weight of the virus is proportional to its length, the molecular weight of the M13 mutants is $M=M_{wt}L/L_{wt}$, with $M_{wt}=1.64\times10^7$ g/mol equal to the molecular weight of wild type M13. Virus production is explained elsewhere [29]. Two of the length mutants (0.64 and 0.39 μm) were grown using the phagemid method [16,29], which produces bidisperse solutions of the phagemid and the 1.2 μm helper phage. Sample polydispersity was checked using agarose gel electrophoresis on the intact virus, and on the viral DNA. Excepting the phagemid solutions which were 20% by mass 1.2 μm helper phage, virus solutions were highly monodisperse as indicated by sharp electrophoresis bands [21]. All of these virus suspensions form well defined smectic phases [16].

All samples were dialyzed against a 20 mM Tris-HCl buffer at *p*H 8.2 or 20 mM sodium acetate buffer adjusted with acetic acid to *p*H 5.2. To vary ionic strength, NaCl was added to the buffering solution. The linear surface charge density of *fd* is approximately 10 e^-/nm $(3.4\pm0.1$ e^-/coat protein) at *p*H 8.2 and 7 e^-/nm $(2.3\pm0.1$ e^-/coat protein) at *p*H 5.2 [19]. The M13 surface charge is 7 e^-/nm $(2.4\pm0.1$ e^-/coat protein) at *p*H 8.2 and 3.6 e^-/nm $(1.3\pm0.1$ e^-/coat protein) at *p*H 5.2 as determined by comparing the M13 composition and electrophoretic mobilities to those of *fd* [21]. On the viral surface, *fd* has four negatively ionizable amino acids and one positively ionizable amino acid per coat protein. At neutral *p*H, the terminal amine contributes approximately $+1/2e$ charge. The M13 surface has three negatively ionizable amino acids, one positively ionizable amino acid and the terminal amine $(+1/2e)$ per coat protein.

After dialysis, the virus suspensions were pelleted using ultracentrifugation at $200\,000\times$g for 3 h. The supernatant was discarded and the pellet resuspended in buffer overnight. The amount of buffer added was selected so that the suspension concentration was just greater than the *N-S* transition. Virus suspensions were then allowed to equilibrate to room
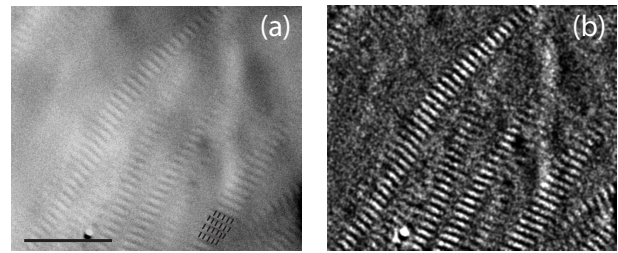

FIG. 2. (a) DIC microscopy image of nematic-smectic coexistence of *fd* virus suspensions. The smectic phase can be recognized by the ladderlike structures. The periodicity of the bands corresponds to one virus length. Virus rods are oriented perpendicular to the layers as illustrated. The uniform texture is the nematic phase. (b) Digitally enhanced image of (a). The scale bar is 10 μm.

temperature. Bulk separation of the nematic and smectic phases is not observed, perhaps because of the high viscosity of the suspensions near the *N-S* transition. However, the phase transition is clearly first order as smectic or nematic domains can be observed using differential interference contrast microscopy (DIC, 60X water immersion lens, Nikon) in coexistence with predominantly nematic and smectic bulk phases, respectively. Typically, coexistence is observed as ribbons of smectic phase reaching into a nematic region, as shown in Fig. 2.

The measurements of the *N-S* phase boundary (Figs. 3 and 5) exhibit a large amount of scatter. There are several factors which contribute to the difficulty of determining the smectic phase diagram. First, identifying the smectic phase is surprisingly difficult using bulk properties. Specifically, the pellets we prepare by centrifugation, which have a concen-
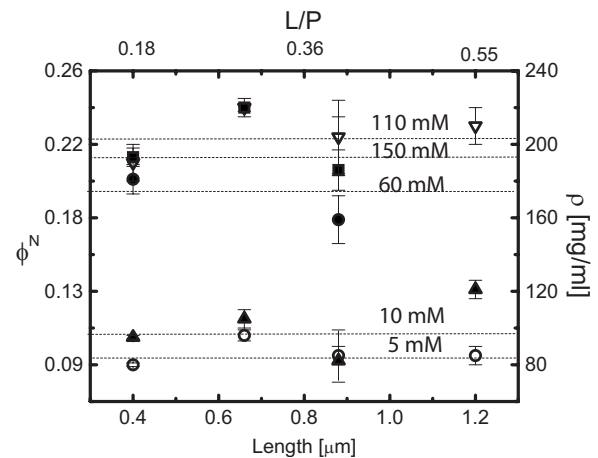

FIG. 3. Coexisting nematic volume fraction at the nematic-smectic phase transition, ϕ^N, for multiple ionic strengths at *p*H 8.2 as a function of rod length L and flexibility L/P. On the right axis is the measured concentration in mass density $\rho^N=\phi^N M/vN_a$, where N_a is Avagadro's number. Legend for ionic strengths is as follows: ○ 5 mM, ▲ 10 mM, ● 60 mM, ▽ 110 mM, ■ 150 mM. With increasing ionic strength ϕ^N increases due to increasing electrostatic screening. Dashed lines are a guide to the eye at constant ionic strength. Within experimental accuracy, the smectic phase transition is independent of flexibility within the measured range of $0.18<L/P<0.54$.

tration far exceeding the smectic phase boundary (about 300 mg/ml), are not iridescent. Only upon dilution of the pellet to a concentration within 10% of the *N-S* transition does iridescence appear [8]. Complicating matters is that sometimes samples are strongly iridescent, but sometimes iridescence is weak. This makes the nematic-smectic boundary hard to distinguish. In past experiments, the motion of fluorescently labeled individual virus tracer particles in both nematic and smectic phases was observed at the single particle level [30]. In the nematic phase the labeled tracer viruses execute Brownian motion and diffuse back and forth parallel to their long axis. Rotational diffusion and diffusion perpendicular to their long axis is absent. In the smectic phase, the labeled virus appear immobile. We assume the virus diffuses perpendicular to their diameter, but to the eye this motion is not apparent. The vanishing of interlayer diffusion (and the associated divergence in viscosity) at the nematic to smectic phase transition is expected [23], but it may account for the lack of iridescence in the centrifuged pellets. Perhaps during centrifugation the virus is concentrated too rapidly for the smectic layers to form and a nematic glass is formed instead.

The high viscosity also contributes to measurement error. First, the samples do not mix well and the concentration may not be homogeneous. Second, high viscosity prevents bulk phase separation of the samples. Gentle centrifugation did not induce the smectic regions to separate from the nematic. This may also imply that the density of the smectic and nematic are similar. Because bulk phase separation does not occur, we cannot accurately identify the relative percentages of the nematic and smectic phases within a coexisting sample. Consequently, we measure an average concentration of the nematic and smectic phases weighted by the percentage of coexisting nematic and smectic phases in the coexistence region. But since we can not precisely control the percentage of coexisting phases, this results in spread in the phase boundary measurement.

To minimize the uncertainty in measurements of the coexistence concentrations the following protocol was implemented. After the concentrated pellets were resuspended, they were systematically diluted until bright iridescence was observed (usually observed as a thin iridescent film coating the walls and meniscus of the sample in the centrifuge tube). For illumination we used a collimated light source with a 20 W tungsten bulb, although a simple flashlight also works well [31,32]. To create iridescence we illuminated and viewed the sample at low angle according to the Bragg condition; $2d = \lambda \sin \theta$. If iridescence was observed we confirmed the presence of the smectic by examining small amounts of the bulk sample in an optical microscope using high resolution DIC optics as shown in Fig. 2. The location of the *N-S* transition was bracketed by measuring the highest nematic volume fraction for which no iridescence was observed (ϕ^N) and the lowest volume fraction (ϕ^S) for which the sample was 100% smectic. 100% smectic samples were defined to be entirely iridescent, and when examined in the microscope, contained no observable nematic domains.

The volume fraction ϕ^S is defined as $c^S v$, where c^S is the number density and v is the volume of a single rod $\pi L D^2 / 4 = 3 \times 10^{-17}$ [cm^3]. A similar equation holds for ϕ^N.

An alternative measure of the volume of a single rod is obtained from the molecular weight and mass density of the virus as $v_m = M/(N_A \rho_o) = 2 \times 10^{-17}$ [cm^3]. The volume v_m represents the volume of water displaced by the virus. It is not too surprising that $v_m < v$ because fd is a hollow protein cylinder partially filled with DNA and therefore the volume of displaced fluid is less than the volume circumscribed by the outer dimensions of the hollow virus. In calculating the volume fraction, it is appropriate to use v and not v_m.

Because it was difficult to ensure that a sample was 100% smectic near the coexistence region, the majority of the data presented here is of ϕ^N, which can be identified accurately by the absence of both smectic layers and iridescence. For some samples, ϕ^S could be pinpointed, and using those samples we estimated the width of the coexistence region. Those results are presented at the end of the Sec. IV. The concentration of the phases was measured by absorption spectroscopy with the optical density (A) of the virus being $A^{1 \text{ mg/ml}}_{269 \text{ nm}} = 3.84$ for a path length of 1 cm.

Since knowing the surface charge of the virus is critical to our analysis of the *N-S* transition, we experimentally measured the *p*H of the virus solutions at concentrations in the nematic phase just below the *N-S* transition. We found that for an initial buffer solution at *p*H 8.2 (Tris-HCl buffer *p*Ka=8.2), the *p*H of the concentrated virus suspensions is slightly less than 8.2, but still well within the buffering *p*H range (*p*H=*p*Ka±1). The surface charge does not change significantly over this range [19]. At *p*H 5.2 (acetic acid buffer *p*Ka=4.76) the measured *p*H of the virus suspensions near the *N-S* transition was slightly higher than 5.2, with *p*H increasing slightly with decreasing ionic strength, most likely due to the relatively high concentration of virus counterions (50–100 mM) as compared to buffer ions (20 mM). However, this shift away from the *p*Ka has little influence on the phase behavior.

IV. RESULTS AND DISCUSSION

A. Flexibility and ionic strength dependence of the *N-S* transition

Figure 3 shows ϕ^N as a function of the M13 mutant particle length, and therefore virus flexibility by L/P, for multiple ionic strengths. Focusing on how rod flexibility influences the phase transition, we observe that at each ionic strength the measured ϕ^N is independent of virus length, within experimental accuracy, and thus independent of flexibility in the range of $0.18 < L/P < 0.54$. We also observe that with increasing ionic strength, and thus increased screening of electrostatic interactions, the volume fraction of the phase transition increases. This increase in phase transition concentration with ionic strength is consistent with previous measurements for suspensions of fd virus [8]. The bidispersity of the 0.64 μm and 0.39 μm rod suspensions does not seem to influence the phase boundary because these samples, which are 20% 1.2 μm rods by mass, exhibit the same phase behavior as samples which are 100% 1.2 μm rods.

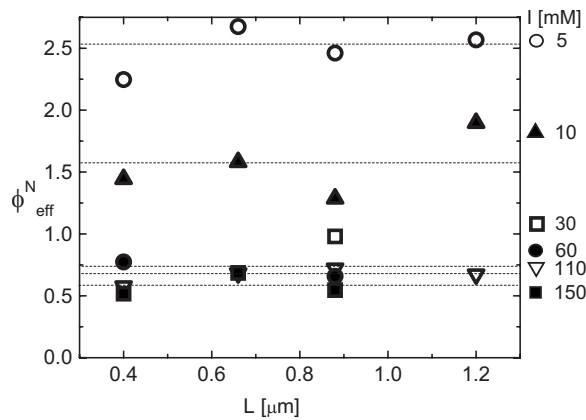The nematic-smectic transition of flexible, hard rods has been studied both theoretically and computationally

FIG. 4. Effective nematic volume fraction at the nematic-smectic phase transition $\phi_{\text{eff}}^N = \phi^N (D_{\text{eff}}^N)^2/D^2$ for multiple ionic strengths at pH 8.2 as a function of L. ϕ^N, the actual nematic volume fraction at the N-S transition, is shown in Fig. 3. Legend for symbols is to the right of the figure. Dashed lines drawn are a guide to the eye and are at constant ionic strength. Because ϕ_{eff}^N strongly depends on ionic strength, we conclude that D_{eff}^N does not accurately describe the electrostatic interactions at high virus concentrations.

[3,9,10,33]. A small amount of flexibility is expected to drive the smectic phase to higher concentrations, ranging from the predicted hard, rigid rod concentration of $\phi^N = \phi^{N*} \times \phi^{CP}$ $=0.43$, where $\phi^{N*} = 0.47$ and ϕ^{CP} is the closed packed volume fraction of infinitely long spherocylinders $\phi^{CP} = 0.907$ [2], to approximately $0.75 \lesssim \phi^N \lesssim 0.8$ within the semiflexible limit [9]. Within the semiflexible limit ($L/P \sim 1$), however, ϕ^N is predicted to be essentially independent of flexibility [9]. This insensitivity of ϕ^N to flexibility in the semiflexible limit is in agreement with the measurements presented in Fig. 3. We note that this result is in striking contrast to the significant flexibility dependence measured at isotropic-nematic transition for this same system of semiflexible M13 mutants which we describe in a separate report [21].

Two methods for incorporating electrostatics into the N-S phase transition of hard rods were described earlier in this paper [7,20,24]. One way to compare our results with hard-rod theories is to graph ϕ_{eff}^N, the measured effective volume fraction along the nematic-smectic transition, and compare it to the theoretical volume fraction, $\phi_{\text{th}}^N = 0.75$, for the N-S transition of hard, semiflexible rods [3,9]. ϕ_{eff}^N is defined as $c^N \pi L (D_{\text{eff}}^N)^2/4 = \phi^N (D_{\text{eff}}^N)^2/D^2$, where D_{eff}^N is Onsager's effective diameter within the nematic phase, and is shown in Fig. 4 for the data presented in Fig. 3. If the effect of electrostatics can be accounted for by replacing D with D_{eff}^N, as can be done at the isotropic-nematic transition at high ionic strength, we could predict that $\phi_{\text{eff}}^N = \phi_{\text{th}}^N = 0.75$. In other words, if D_{eff}^N accurately models the interparticle electrostatic interactions, the effective volume fraction ϕ_{eff}^N should be equivalent to the hard-flexible rod volume fraction and should be independent of ionic strength. Thus multiplying the measured values for ϕ^N shown in Fig. 3 by $(D_{\text{eff}}^N)^2/D^2$ should result in the collapse of all the different ionic strength data.

In Fig. 4, however, we clearly observe an ionic strength dependence in ϕ_{eff}^N, with ϕ_{eff}^N ranging from 0.5 to 2.5. Previ-
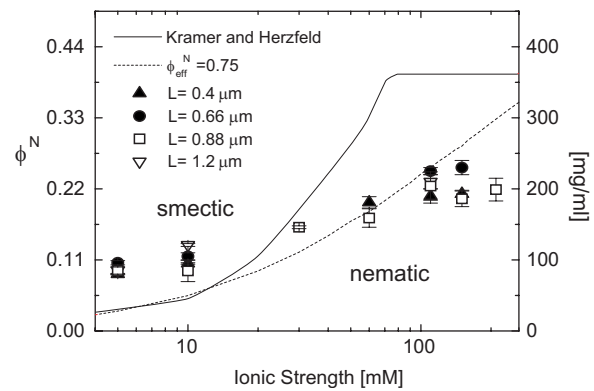

FIG. 5. (Color online) ϕ^N for each of the four M13 length mutants as a function of ionic strength at pH 8.2. The solid line is ϕ^N taken from calculations by Kramer and Herzfeld [7] for the N-S transition of particles the same size as fd and with a renormalized surface charge of $1\, e^-/7.1$ Å. The dashed line is ϕ^N $= \phi_{\text{eff}}^N * D^2/(D_{\text{eff}}^N)^2$ with $\phi_{\text{eff}}^N = \phi_{\text{th}}^N = 0.75$.

ously, we observed $\phi_{\text{eff}}^N = 0.75$ independent of ionic strength for suspensions of wild type fd virus [8]. The data in Fig. 4 is consistent with the previous measurements only in the range of ionic strengths from 60 to 110 mM. In this paper, as a result of extensive measurements of the smectic phase boundary as a function of virus length, we find that ϕ_{eff}^N tends to be less than 0.75 for $I > 100$ mM and greater than 0.75 otherwise. From these observations we conclude that D_{eff}^N overestimates the electrostatic interactions at low ionic strength, and underestimates them at high ionic strength.

To better understand the ionic strength dependence of the phase transition, the experimental ϕ^N is compared to the theoretical expression $\phi_{\text{eff}}^N = 0.75$ as a function of ionic strength in Fig. 5. Both ϕ^N and $\phi_{\text{eff}}^N = 0.75$ increase with increasing ionic strength, indicating that D_{eff}^N is qualitatively correct in describing the electrostatic interactions. However, the ionic strength dependence of the N-S boundary predicted by D_{eff}^N is much greater than what is measured. This contrasts with the I-N transition, where D_{eff} quantitatively incorporates the electrostatic interactions between virus rods at high ionic strength [21], as shown in Fig. 1. The observation that ϕ_{eff}^N only qualitatively describes the ionic strength dependence of the N-S phase transition is not surprising because D_{eff}^N is based on the second virial approximation which, strictly speaking, is valid only for isotropic suspensions at low concentrations.

A second method for incorporating electrostatics into hard-rod theory developed by Kramer and Herzfeld is also presented in Fig. 5. As with D_{eff}^N, Kramer and Herzfeld's avoidance model predicts an increase in ϕ^N with increasing ionic strength. However, the avoidance model predicts an even steeper slope in the phase transition concentration with increasing ionic strength than Onsager's D_{eff}. Furthermore, it predicts a saturation of ϕ^N at a value of 0.39 above ~ 80 mM, similar to the theoretical value for hard, rigid spherocylinders $\phi^N = 0.43$ [2,7]. Indications of the ionic strength independence of ϕ^N are observed experimentally for $I > 100$ mM, but the avoidance model over-predicts the transition concentrations by a factor of 2. The significant differ-

ence in ionic strength dependence between the experimental results and both available theories suggests that more theoretical and computational work is needed to understand the mechanism behind the *N-S* phase behavior of charged, flexible rods.

One possible reason for the discrepancy between our measurements and the predicted $\phi_{th}^N=0.75$ for hard-flexible rods may be due to a coupling of the electrostatic and fluctuation induced repulsion [34]. This coupling may produce an inter-rod repulsion which is a complex combination of flexible-hard rod and charged-rigid rod interactions. It has been shown for concentrated suspensions of DNA that fluctuations due to the flexibility of the DNA actually enhance inter-rod repulsions in an exponential manner [35,36]. The consequence is that for a given osmotic pressure exerted by a concentrated DNA suspension, the volume fraction of DNA is much lower than predicted by Poisson-Boltzmann electrostatics alone. This hypothesis is consistent with our measurements at high ionic strength where ϕ^N which is much lower than predicted by renormalizing ϕ^N by $(D_{eff}^N)^2/D^2$ alone, but further theoretical work is needed to better understand the influence of both charge and flexibility on the *N-S* transition.

B. Surface charge dependence of the *N-S* transition

The nonlinearity of the Poisson-Boltzmann equation predicts that for high linear charge density the long-range electrostatic potential between rods is insensitive to the magnitude of the surface charge and thus the *N-S* boundary should be insensitive to *p*H as long as the virus remains highly charged [1,23]. This is confirmed at the isotropic-nematic transition, where the charge dependence is well described by D_{eff} and the *p*H dependence of the phase transition is very small [21]. To determine the influence of changing virus surface charge on *N-S* phase transition, we measured the phase behavior of *fd* and M13 at both *p*H 8.2 and *p*H 5.2 and as a function of ionic strength [Figs. 6(a) and 6(b)]. At low ionic strength we find a clear *p*H dependence of the *N-S* transition for both M13 and *fd* suspensions: suspensions at higher *p*H (higher surface charge) consistently enter a smectic phase at lower concentrations. At high ionic strength, however, the *p*H dependence of ϕ^N vanishes, in agreement with previous observations that the electrostatic interactions are better described by D_{eff} at high ionic strength. In Fig. 6(c) we compare the ionic strength dependence of ϕ^N for M13 and *fd* suspensions when both viruses have the same surface charge of 7 e^-/nm. While the rods have the same total surface charge, the location of the charges (positive and negative) on the surface differs between the two viruses. We find that the phase diagrams for M13 and *fd* are similar when they share the same surface charge, as expected.

In Fig. 7 we plot the effective volume fraction, ϕ_{eff}^N, of the *fd* and M13 suspensions shown in Figs. 6(a) and 6(b), respectively, as a function of ionic strength. Because the virus is highly charged and in the condensation limit we would predict that by scaling ϕ^N by $(D_{eff}^N)^2/D^2$, the effective volume fraction for rods of different surface charges would be identical. At high ionic strength we find this is indeed true; ϕ_{eff}^N for suspensions at *p*H 5.2 and *p*H 8.2 are in excellent
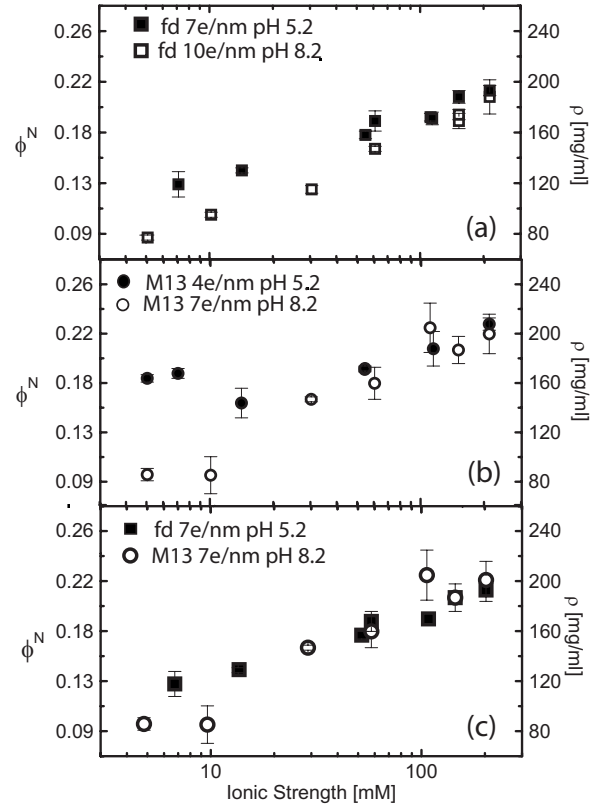

FIG. 6. Nematic volume fraction ϕ^N at the nematic-smectic phase transition as function of ionic strength for suspensions of (a) *fd* and (b) M13 at *p*H 5.2 (solid) and *p*H 8.2 (open). (c) shows M13 (*p*H 8.2) and *fd* (*p*H 5.2) at 7 *e*/nm surface charge.
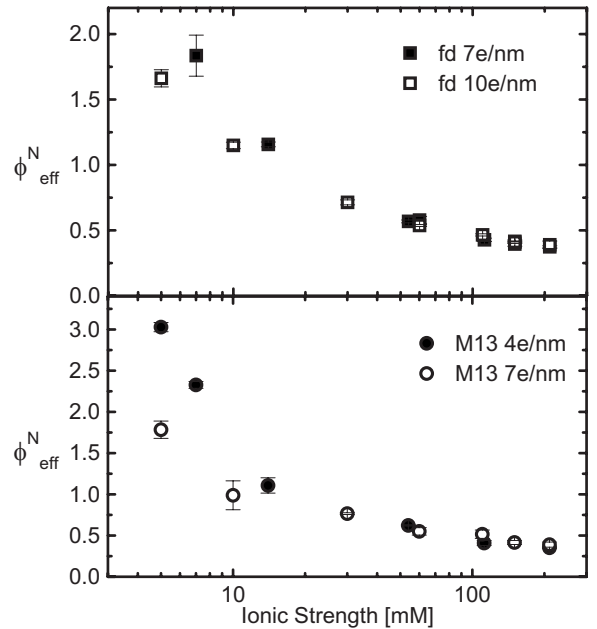

FIG. 7. Effective nematic volume fraction at the nematic-smectic phase transition $\phi_{eff}^N=\phi^N(D_{eff}^N)^2/D^2$ as function of ionic strength for suspensions of (a) *fd* and (b) M13 at *p*H 5.2 (solid) and *p*H 8.2 (open).
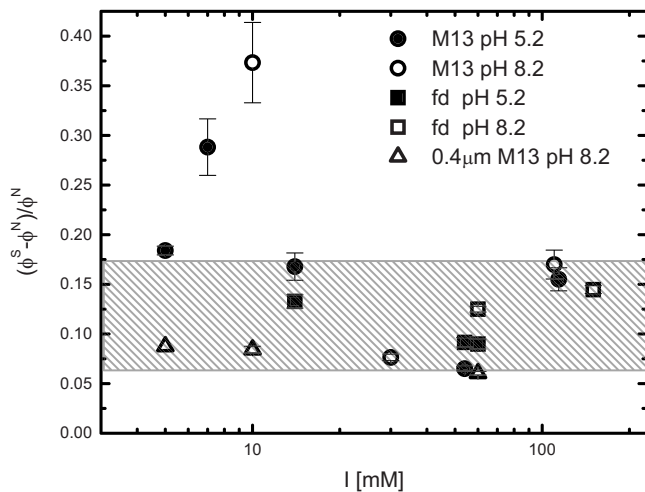
FIG. 8. The width of the coexistence region $[(\phi^S - \phi^N)/\phi^N]$ of the nematic-smectic transition for suspensions of M13 at pH 8.2 and 5.2, fd at pH 8.2 and 5.2, and 0.4 μm M13 mutant at pH 8.2. Hashed area illustrates the range of coexistence widths measured. The averaged value of the coexistence width is 0.12±0.5, independent of virus type.

agreement with each other. However, at low ionic strength there is a small pH dependence in the measured values of ϕ_{eff}^N for both M13 and fd. As discussed previously, if the scaling argument is correct then ϕ_{eff}^N should be independent of ionic strength as well as of pH. In Fig. 1 it was demonstrated that this scaling works well for the I-N phase transition at high ionic strength and has at most a 30% variation in scaled concentration at low ionic strength. This is in contrast to the N-S transition, where the scaled concentrations of M13 vary by as much as 600%. Clearly, the scaling of the hard rod diameter D by the effective diameter D_{eff}, a technique which works so well for the I-N transition, fails for the N-S transition.

C. Nematic-smectic coexistence region

The width of the nematic-smectic coexistence region was also measured for multiple virus suspensions as a function of length, ionic strength, and pH. In Fig. 8 we present representative measurements of the coexistence widths for some of the viral suspensions. These samples were chosen because they represent the data with the largest number of data points within the coexistence region. The coexistence region was found by mapping the range of concentrations in which both smectic and nematic phases were observed, using the characteristics listed in Sec. III. We found that the width of the coexistence region $(\phi^S - \phi^N)/(\phi^N) \sim 0.12 \pm 0.05$, independent of rod length (rod flexibility), solution pH (rod surface charge), and ionic strength. By knowing that the coexistence width is approximately $0.12 \times \phi^N$ independent of viral sus-

pension, we can subsequently determine ϕ^S and therefore have a measure of the whole nematic-smectic phase transition region. The width of the coexistence region for the 0.4 μm rods was 0.08±0.01, which suggests that the shorter, more rigid, rods may have a smaller coexistence width than the 0.88 μm fd and M13 rods. This is consistent with the observation that TMV, a rigid virus, has a second order N-S transition [37]. However, the measurement of the coexistence width is quite noisy due to the difficulty in measuring ϕ^S, making the length dependence of the coexistence width difficult to accurately determine.

Theoretically, there are few predictions for the width of the coexistence region, though it has been shown in simulations of hard flexible rods that the phase transition is indeed first order [3], and that the discontinuous nature of the phase transition is strengthened for flexible rods [9]. Predicted coexistence widths range from ∼0.08 in simulations of flexible rods [3], to ∼0.18 for parallel hard-spherocylinder theory [7]. Both of these numbers are consistent with our measurements.

V. CONCLUSION

We have examined the nematic-smectic phase transition for charged, semiflexible virus rods as a function of length, surface charge, and ionic strength. We found that within the semiflexible-rod limit the N-S phase boundary is independent of rod flexibility, as predicted theoretically. The width of the N-S coexistence region is also independent of rod flexibility, within our experimental accuracy, and is equal to 12% of the nematic coexistence concentration. By measuring the ionic strength and charge dependance of this transition we observed the failure of mapping the charged rods onto a hard-rod model. The charge and ionic strength dependent effective diameter, D_{eff}, calculated using Onsager's second virial approximation overestimates the electrostatic interactions at low ionic strength, and underestimates them at high ionic strength.

We hypothesize that the discrepancy between our measurements of the N-S transition concentration and the predicted transition concentration for hard-flexible rods ($\phi_{eff}^N = 0.75$) may be due to the coupling of flexible-hard rod repulsion and electrostatic repulsion. Experimental tests of this hypothesis could be made by measuring M13 and fd equations of state (pressure vs density), and thus the particle-particle interactions, as a function of solution salt and pH, as in techniques developed for DNA [35]. Theoretically, this hypothesis can be tested by extending previous theory to include the nematic-smectic transition [35].

[1] L. Onsager, Ann. N.Y. Acad. Sci. **51**, 627 (1949).

[2] P. G. Bolhuis and D. Frenkel, J. Chem. Phys. **106**, 666 (1997).

[3] J. M. Polson and D. Frenkel, Phys. Rev. E **56**, R6260 (1997).

[4] R. B. Meyer, in *Dynamics and Patterns in Complex Fluids*, edited by A. Onuki and K. Kawasaki (Springer-Verlag, Berlin, 1990), p. 62.

[5] S. Fraden, in *Observation, Prediction, and Simulation of Phase Transitions in Complex Fluids*, edited by M. Baus, L. F. Rull, and J. P. Ryckaert (Kluwer Academic, Dordrecht, 1995), pp. 113–164.

[6] H. Maeda and Y. Maeda, Phys. Rev. Lett. **90**, 018303 (2003).

[7] E. M. Kramer and J. Herzfeld, Phys. Rev. E **61**, 6872 (2000).

[8] Z. Dogic and S. Fraden, Phys. Rev. Lett. **78**, 2417 (1997).

[9] A. V. Tkachenko, Phys. Rev. Lett. **77**, 4218 (1996).

[10] P. van der Schoot, J. Phys. II **6**, 1557 (1996).

[11] R. Podgornik, H. Strey, and V. Parsegian, Curr. Opin. Colloid Interface Sci. **3**, 534 (1998).

[12] F. Livolant, A. Levelut, J. Doucet, and J. Benoit, Nature (London) **339**, 724 (1989).

[13] A. Grosberg and A. Khokhlov, *Giant Molecules: Here, There and Everywhere* (Academic Press, New York, 1997).

[14] J. Lapointe and D. A. Marvin, Mol. Cryst. Liq. Cryst. **19**, 269 (1973).

[15] J. Tang and S. Fraden, Liq. Cryst. **19**, 459 (1995).

[16] Z. Dogic and S. Fraden, Philos. Trans. R. Soc. London, Ser. A **359**, 997 (2001).

[17] P. G. de Gennes and J. Prost, *The Physics of Liquid Crystals*, 2nd ed. (Oxford Science, Oxford, U.K., 1993).

[18] D. A. Marvin, R. D. Hale, C. Nave, and M. H. Citterich, J. Mol. Biol. **235**, 260 (1994).

[19] K. Zimmermann, J. Hagedorn, C. C. Heuck, M. Hinrichsen, and J. Ludwig, J. Biol. Chem. **261**, 1653 (1986).

[20] A. Stroobants, H. N. W. Lekkerkerker, and T. Odijk, Macromolecules **19**, 2232 (1986b).

[21] K. R. Purdy and S. Fraden, Phys. Rev. E **70**, 061703 (2004).

[22] Z. Y. Chen, Macromolecules **26**, 3419 (1993).

[23] A. Stroobants, H. N. W. Lekkerkerker, and D. Frenkel, Phys. Rev. Lett. **57**, 1452 (1986a).

[24] G. J. Vroege and H. N. W. Lekkerkerker, Rep. Prog. Phys. **55**, 1241 (1992).

[25] K. R. Purdy, Z. Dogic, S. Fraden, A. Rühm, L. Lurio, and S. G. J. Mochrie, Phys. Rev. E **67**, 031708 (2003).

[26] M. A. Cotter and D. C. Wacker, Phys. Rev. A **18**, 2669 (1978).

[27] M. A. Cotter, in *The Molecular Physics of Liquid Crystals*, edited by G. R. Luckhurst and G. W. Gray (Academic Press, London, 1979), pp. 169–189.

[28] S. A. Berkowitz and L. A. Day, J. Mol. Biol. **102**, 531 (1976).

[29] J. Sambrook, E. F. Fritsch, and T. Maniatis, *Molecular Cloning: A Laboratory Manual*, 2nd ed. (Cold Spring Harbor Laboratory, New York, 1989).

[30] M. Lettinga, E. Barry, and Z. Dogic, Europhys. Lett. **71**, 692 (2005).

[31] C. Wetter, Biol. Unserer Zeit **3**, 81 (1985).

[32] U. Kreibig and C. Wetter, Z. Naturforsch. A **35c**, 750 (1980).

[33] R. C. Hidalgo, D. E. Sullivan, and J. Z. Y. Chen, Phys. Rev. E **71**, 041804 (2005).

[34] T. Odijk, Biophys. Chem. **46**, 69 (1993).

[35] H. H. Strey, V. A. Parsegian, and R. Podgornik, Phys. Rev. Lett. **78**, 895 (1997).

[36] H. H. Strey, V. A. Parsegian, and R. Podgornik, Phys. Rev. E **59**, 999 (1999).

[37] J. H. Wang, F. Lonberg, X. Ao, and R. B. Meyer, in *Ordering in Macromolecular Systems*, edited by A. Teramoto, M. Kobayashi, and T. Norisuje (Springer-Verlag, Berlin 1994).